ADVANCED MATERIALS
www.advmat.de

Kirigami-Based Light-Induced Shape-Morphing and Locomotion

Yu-Chieh Cheng, Hao-Chuan Lu, Xuan Lee, Hao Zeng,* and Arri Priimagi*

The development of stimuli-responsive soft actuators, a task largely undertaken by material scientists, has become a major driving force in pushing the frontiers of microrobotics. Devices made of soft active materials are oftentimes small in size, remotely and wirelessly powered/controlled, and capable of adapting themselves to unexpected hurdles. However, nowadays most soft microscale robots are rather simple in terms of design and architecture, and it remains a challenge to create complex 3D soft robots with stimuli-responsive properties. Here, it is suggested that kirigami-based techniques can be useful for fabricating complex 3D robotic structures that can be activated with light. External stress fields introduce out-of-plane deformation of kirigami film actuators made of liquid crystal networks. Such 2D-to-3D structural transformations can give rise to mechanical actuation upon light illumination, thus allowing the realization of kirigami-based light-fuelled robotics. A kirigami rolling robot is demonstrated, where a light beam controls the multigait motion and steers the moving direction in 2D. The device is able to navigate along different routes and moves up a ramp with a slope of 6°. The results demonstrate a facile technique to realize complex and flexible 3D structures with light-activated robotic functions.

Soft robots are machines composed of actuating elements based on flexible materials, whose moduli typically lie in the same range as in biological systems (10^4–10^9 Pa).[1] Being soft, they are expected to offer safe contact with human body or with fragile objects during manipulation.[2] Their flexibility, in turn, brings about additional degrees of freedom in robotic movements, leading to adaptation to hurdles encountered in various environments.[3] In the past decades, stimuli-responsive soft material systems have attained an increasing amount of interest. The interest stems from novel possibilities to design and fabricate soft devices with miniaturize sizes and ever-more-complex functions.[4,5] Among the wealth of stimuli-responsive materials, carbon-based bilayers,[6] liquid crystal elastomers and polymer networks (LCNs),[7] hydrogels,[8] and magnet-doped rubbers[9] stand out as prominent candidates for soft microrobotics. The devices composed of these materials adopt novel control strategies, shifting from conventional wire-connections (electrically or via pneumatic tubes)[10,11] to a wireless approach relying on external energy sources such as magnetic fields,[12] light fields,[13] humidity,[14] or chemical reactions.[15] When exposed to stimuli, the specific form of deformation can be programmed by tuning molecular orientation, stiffness gradient or structural anisotropy.[16]

Liquid crystal polymer networks (LCNs) are crosslinked polymers that combine the anisotropy arising from oriented liquid crystalline mesogens and the elasticity of the polymer network.[17,18] Their versatile deformabilities upon heat/light stimuli give rise to a fast-increasing interest in realization of novel soft robotic systems, in which the nature-inspired strategies are often adopted. Strips mimicking opening and closing of seedpods and flowers,[19,20] actuators exhibiting caterpillar-like motion such as rolling,[21] inching[22] and travelling-wave movement,[23] swimmers mimicking microzooplankton,[24] and snail-like crawlers[25] are but few examples. Due to restrictions in sample size (below few centimeters) and lack of actuation complexity, such soft actuators are based on simple architectures with limited degrees of freedom in movement. To obtain soft microrobots that better mimic their natural counterparts, realization of complex 3D architectures, needed for versatile actuation, is in great demand.

To achieve 3D robotic structures in LCNs, laser writing and ink-jet printing have been investigated.[26–28] For example, light-fueled walkers[26] and tunable lenses[28] are realized across microscopic and macroscopic length scales. However, to successfully use these techniques, the monomer mixture as well as polymerization conditions have to be carefully optimized. In addition, LCNs also pose additional challenges due to the need for precise molecular alignment control, and complications (due to, e.g., swelling) that may arise during the development process. These limitations restrict the generality of these

Prof. Y.-C. Cheng, H.-C. Lu, X. Lee
Department of Electro-Optical Engineering
National Taipei University of Technology
10608 Taipei, Taiwan
E-mail: yu-chieh.cheng@ntut.edu.tw
Dr. H. Zeng, Prof. A. Priimagi
Smart Photonic Materials
Faculty of Engineering and Natural Sciences
Tampere University
P. O. Box 541, FI-33101 Tampere, Finland
E-mail: hao.zeng@tuni.fi
The ORCID identification number(s) for the author(s) of this article can be found under https://doi.org/10.1002/adma.201906233.

DOI: 10.1002/adma.201906233

techniques in the context of LCNs and block their widespread use with more versatile monomer options. Hence, it would be extremely useful to have a facile 3D fabrication technique that would circumvent these limitations, and could be used with many different classes of stimuli-responsive materials.

While trying to address the above challenge, we were first inspired by the art of paper folding—also called origami—a technique to transform a 2D material sheet into a complex, predesigned 3D sculpture.[29–31] This concept has been used in fabricating autofolding structures and self-assembled nanodevices.[32–34] Very recently, research trends in the field have focused on soft responsive materials to obtain origami geometries while maintaining the reversibility in shape morphing.[35] However, unlike in inelastic materials such as paper, obtaining sharp, well-defined hinges in soft material sheets is challenging. Hence, much effort has been put to optimizing the composition of the folded elastic materials.[36]

Soft matter is inherently stretchable, which inspires us to search for other fabrication alternatives. Kirigami, a variation of origami which includes also cutting of the material, requires, in principle, no folding of the structure, and the 2D-to-3D deformation is based on exerting an external force (like stretching) on a precut sheet. Following some simple principles that have been developed in the art of kirigami, a grid-like window for reducing energy consumption,[37] and a walking robot with scale-like skin,[38] have been devised, representing pioneering examples of kirigami robotics based on passive materials. Using stimuli-responsive material sheets with predesigned 2D cut patterns[39] to yield, e.g., stretching, twisting and bending deformations, diverse options of externally controlled 3D structures can be foreseen.

Herein, we suggest that a combination of light-responsive LCN sheets and the kirigami technique can be a useful tool for creating versatile 3D actuators and microrobots with photomechanical movements. For this, a laser engraver is applied to cut kirigami patterns in a photoresponsive thin film based on liquid crystal polymer network (LCN). External stress fields induced by stretching, twisting, and bending are used to trigger out-of-plane deformation in diverse forms to build up different 3D kirigami-based architectures. The same deformations can also be obtained upon light irradiation. We also demonstrate a kirigami-based rolling robot equipped with light-actuated petals to show multigait rolling movement that can be steered forward/backward, navigate along predesigned 2D trajectories, and climb a slope with an inclination up to 6°. We anticipate that kirigami can become a facile technique to obtain complex geometries also in responsive materials other than LCNs, thus providing far-reaching possibilities for soft microdevices with advanced functionalities.

An LCN actuator can response to heat due to the change of molecular alignment/order. By incorporating light-sensitive elements (e.g., photoswitches or photoabsorbers), it can be reshaped through irradiation with specific light wavelength.[40,41] The most common way to fabricate these actuators is to infiltrate a photopolymerizable monomer mixture into a liquid crystal cell with thickness in the range from few to few hundreds of microns (Schematic in **Figure 1**a). In most cases, the inner surfaces of the cell are pretreated, allowing for diverse control over the molecular alignment, and once the mixture is polymerized, the molecular alignment dictates the actuation modes of the resulting LCN.[18] Functional devices that rely on 3D architectures are often realized by integration of strips cut from film-like actuators[42,43] or engineered alignment distribution across the film area to attain versatile out-of-plane buckling.[44]

The monomer mixture used in this study is shown in Figure 1a. We use Dispersed Red 1 (DR1) as a photothermal dye incorporated into the LCN to induce efficient photomechanical movements, alike we have done in several previous studies.[45,46] More details on the fabrication process are given in Experimental Section. The typical mechanical response of an LCN film upon heating and/or illumination is given in Figure S1 in Supporting Information. Our interest toward light-responsive LCN kirigami stems from two reasons. First, soft LCN sheets usually cover an area of a few cm^2, which is ideal for machine engraving or laser cutting. Second, a simple choice of molecular orientation across the film thickness (e.g., splayed or twisted alignment) leads to efficient bending movement of the material. Such "trivial" bending deformation gives rise to nontrivial deformations in the kirigami structures, as will be shown in the following examples.

We implemented a laser engraver to cut a predesigned pattern into the LCN films, as schematically shown in the inset of Figure 1b. When detached from the substrate, a stress field associated with a given external force can induce out-of-plane deformation in such a 2D material sheet. For instance, by lifting up the cut pattern, a flat sheet turns into a 3D ribbon, thus forming a 3D kirigami pattern (Figure 1b). Among the plethora of external force fields applicable for shape morphing, stretching, twisting, and rolling are the most elementary ones. Upon each stress field, the out-of-plane deformation is determined by the cut pattern.

Figure 1c presents three typical kirigami patterns engraved on a splay-aligned LCN film and their 2D-to-3D shape-morphing capabilities by stretching, twisting and rolling. Line-cut patterns are typically used in mechanical metamaterials.[37] Upon in-plane stretching, each cut segment buckles out-of-plane through bending and twisting, thus opening pores of the sheet (Figure 1c-i). In the twisting and rolling modes, since the external forces provide out-of-plane motion, the structures deform along the direction of the stress fields being applied (Figure 1c-ii,iv). In particular, the strips cut perpendicularly to the rolling axis exhibit strain-dependent bending angles (Figure 1d). These kirigami-induced shapes can be further manipulated upon light irradiation, and the dependencies between the structural angles and irradiation intensity are plotted in Figure 1d. Detailed characterization of the strain-induced deformations in kirigami films based on stretching and twisting modes, together with their photomechanical responses, are given in Figures S2 and S3 (Supporting Information). This technique also allows implementation of different kirigami patterns to harvest versatile shape morphing and light actuation capacity, as shown by the examples given in Figures S4–S6 (Supporting Information).

Going beyond shape-morphing and photomechanical actuation we also devised a "rolling LCN kirigami" with light-responsive petals capable of locomotion and light-steered movements. The design principle of the rolling robot is schematically shown in **Figure 2**a, in analogy with paper cutting.

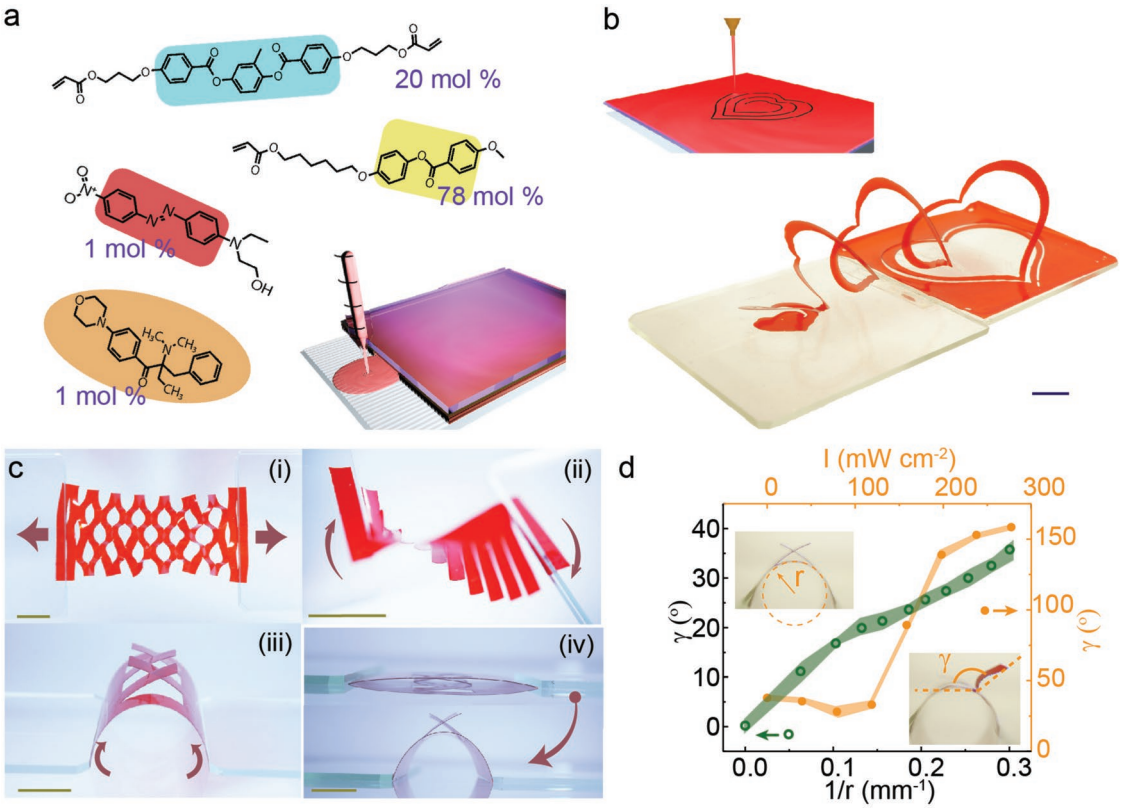

Figure 1. The kirigami concept in stimuli-responsive LCN films. a) Chemical composition of the LC monomer mixture and schematic drawing of the cell infiltration process. b) Photograph of the 2D-to-3D shape-morphing of a kirigami LCN film upon an external stress field. Inset: schematic drawing of laser engraving of corresponding kirigami pattern on the actuating film. c) Three basic deformation modes in LCN kirigami films: stretching (i), twisting (ii), and rolling (iii). iv) The side-view photograph of a cut film upon a rolling deformation. d) Deformation strains upon different stress fields (rolling mode) and illuminating intensities. Error bars indicate standard deviation for $n = 3$ measurements. Insets indicate the bending curvature upon an external force, $1/r$, and the bending angle γ upon light illumination. All scale bars are 5 mm.

Series of stripes with triangular ends are patterned on both sides of a central axis of an LCN film. Each strip is laser cut along the planar direction of the splay-aligned film, and thus able to bend upon light irradiation, forming photomechanical petals for the locomotion. The cut pattern is then rolled up into a tube and reinforced by a plastic ring (for fabrication details and robot dimensions, see Experimental Section). When the petals are illuminated through the substrate (470 nm), they mechanically push the ground and induce sequential robotic motion.

When the robot is set on a flat substrate in the dark, all the petals are inactive, and the whole body is parallel to the ground surface (inset of Figure 2b). To characterize the photomechanical response, we excited one half of the structure through a transparent substrate. Upon illumination, the petals bend toward the substrate, lifting up the center of mass of the structure (Figure 2b), the tilt angle φ depending on the irradiation intensity (Figure 2c; Figure S7, Supporting Information). When the irradiation is ceased, the petals cool down and unbend, retaining the original shape within 2 s, irrespective of irradiation intensity (Figure 2d), as governed by heat dissipation from LCN to the surrounding medium (air). To obtain rolling motion, oblique-incidence illumination through the substrate is required, as shown in Figure 2e. Due to the oblique irradiation, once the bottom petals deform and move the robot forward, the actuated petals roll into dark, cool down, and unbend. In the meantime, a new pair of petals is exposed to light, bending against the ground and moving the robot forward (see the schematic in Figure S8, Supporting Information). A sequence of such events gives rise to continuous rolling with multiple gaits. While switching the incident light direction from left to right, the rolling direction changes (Movie S1, Supporting Information).

To control the movement speed, we set up an optical system to scan the light beam with preselected velocity, and monitored the influence of incidence angle on the rolling motion with an optical set up that is schematically shown in Figure S9 (Supporting Information). The robot position is determined through an image tracking system, with details given in Figure S10 (Supporting Information) and Experimental Section. The moving speed was controlled between 1 and 6 mm s^{-1}. As the robot is driven by step-wise deformation of the petals, the rolling distance, d (solid lines in Figure 2f), is not smoothly following the steadily moving light beam, d_s (dashed lines in Figure 2f), but in an intermittent manner, while failing at the speed of 6 mm s^{-1}. The maximum rolling speed was also affected by light incident angle, θ_{inc}. We measured the mean distance deviation ($\Delta d = d - d_s$) at different scanning speeds and θ_{inc} values, as shown in Figure 2g. Small Δd with minimal standard deviation

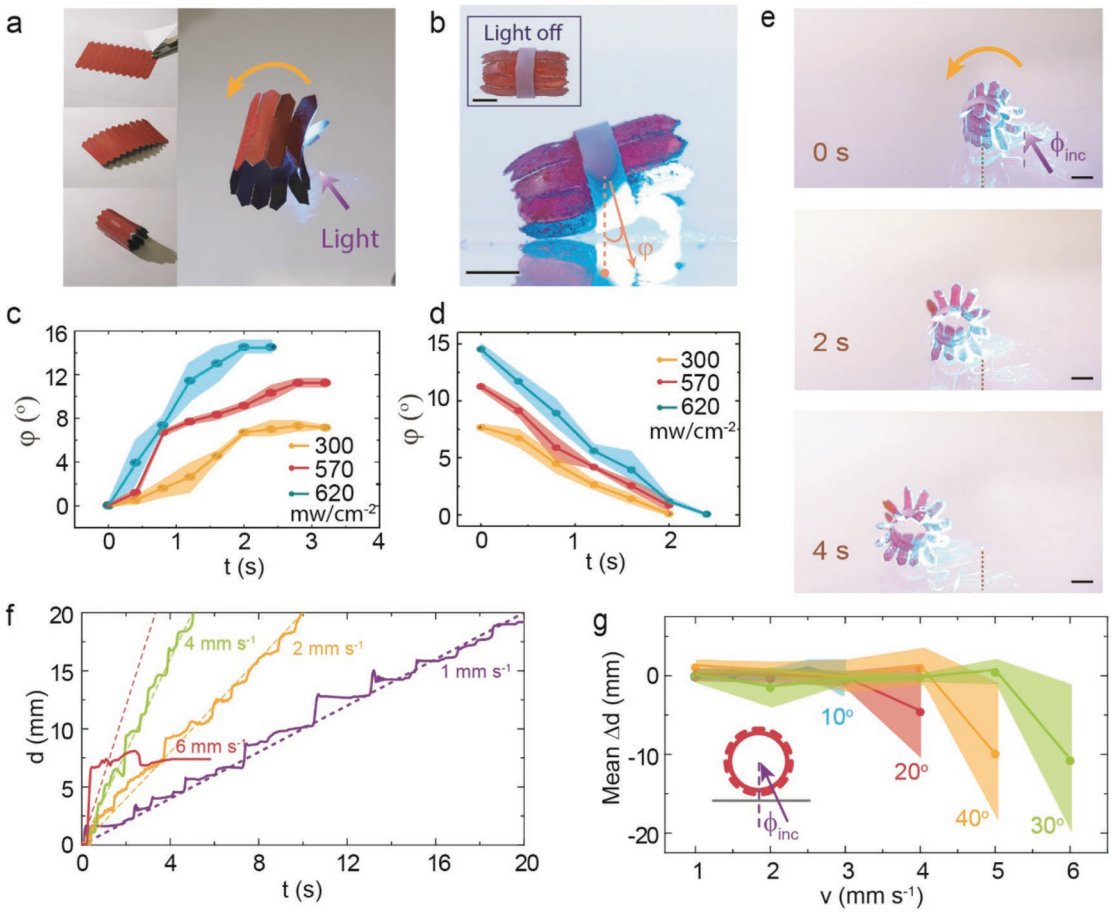

Figure 2. Kirigami-based rolling robot. a) Design of the light-fueled rolling robot. b) Photograph of the robot illuminated (470 nm LED, 570 mW cm^{-2}) on one side of the body to induce tilt (angle φ). Inset shows the same robot in the dark. c) Tilting kinetics at different irradiation intensities and d) retaining the flat state when irradiation is ceased. Error bars in (c) and (d) indicate standard deviation for $n = 3$ measurements. e) Series of photographs showing multigait rolling motion along a straight line by irradiating through the bottom substrate from the direction of the violet arrow. f) The rolling distance d (solid lines) upon scanning the light beam (intensity 620 mW cm^{-2}) with different velocities (solid lines). The dashed lines indicate the steady movement of the light spot. g) The mean distance deviation Δd, between robot and spot position at different scanning speed and incident angles θ_{inc}. The error bars indicate standard deviation for 20 measurements per second for the whole motion period. The data points with maximum error bar values indicate the failure speeds at different incidence angles, where the robot cannot catch up with the spot. Light intensity: 620 mW cm^{-2}. Inset shows the incident angle respect to robot position. All scale bars are 2 mm.

indicates an intermittent movement following the speed of the light spot, while negative Δd with large standard deviation indicates the termination of movement at high scanning speeds. The results in Figure 2g show that the optimal incidence angle is 30°, at which the device reaches a maximum rolling speed of 5 mm s^{-1}. We anticipate this value to be geometry-dependent, and no doubt the maximal speed is strongly affected by material properties, which in turn dictate the actuation and relaxation speed, as well as interaction with the substrate.

The rolling robots in previous reports are based on a single rolled-up tube or spiral ribbons that deform asymmetrically upon light illumination and shadowing.[47,48] The motions of such robots are relatively smooth, as opposed to the one presented in this study, which moves sequentially due to the multi-petal geometry (see Movie S2, Supporting Information). Although a conventional rolling can be more favorable regarding velocity and energy efficiency, the multipetal robot with intermittent motion exhibits a more accurate control in rolling speed and possibility of pin-pointed positioning (Figure 2f,g). Note that although moving intermittently, the robot can reach a relatively high speed of about one body-width (diameter along the moving direction) per second under stationary illumination. But even more importantly, the kirigami structure allows for distinct operation between the left and right petals. This provides additional functionality and enables light-induced steering of the robot movement, a feature that is unreachable in reported rolling robot constructed with a single roll-up tube.

As shown in Figure 2c, the deformation depends strongly on local light intensity. Hence, by tuning the spot position with respect to the center of the structure, one can control the moving direction as illustrated in **Figure 3**a. When the structure is symmetrically irradiated, the petals on both sides undergo similar deformation, yielding forward-rolling motion. When the spot is concentrated to left/right, the petals experiencing stronger light field exhibit larger strains and hence turn the rolling direction into the opposite side (Movie S3, Supporting

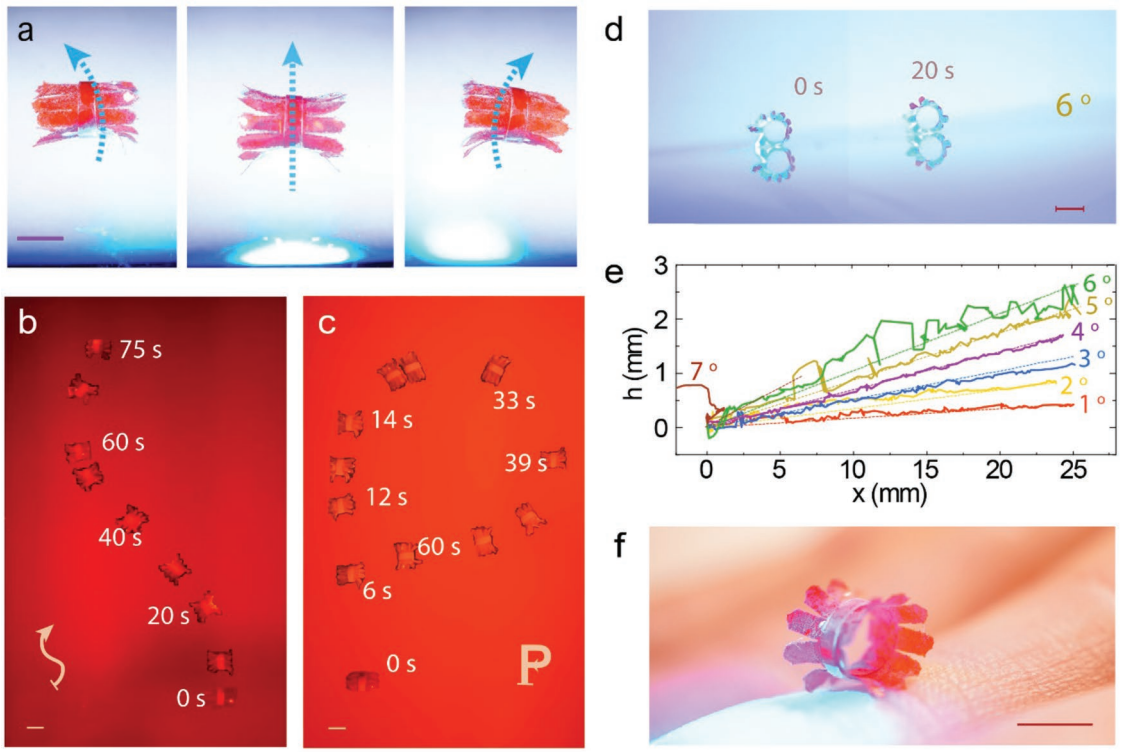

Figure 3. Versatile locomotion of the kirigami-based rolling robot. a) Photographs of the rolling robot turning left, rolling forward and turning right, depending on light excitation direction. b,c) Robot steering along trajectories resembling letters "S" (b) and "P" (c). d) Superimposed images of the robot climbing on a hill with 6° slope. e) Climbing performance of the robot at different slope angles. f) Photograph of the rolling robot when illuminated on human hand. Illumination: 470 nm, 320 mW cm^{-2}. All scale bars are 4 mm.

Information). Based on such capacity, we can manually steer the robot to navigate along predesigned pathways, as shown in Figure 3b,c (see also Movie S4 in the Supporting Information), where trajectories resembling the letters "S" and "P" are achieved, demonstrating versatile 2D control over the robot locomotion.

An inching-type walking robot, that has proper friction bias integrated into the structure, can climb up a slope.[22] However, it is challenging for a symmetric tube to roll up a hill without any external forces. The kirigami robot in this study combines a rolling body and ten pairs of petals and as a result, it can climb a small hill without any structures providing the friction bias. Figure 3e shows the climbing ability at the speed of 1 mm s^{-1}. The central mass position h (in the vertical direction) increases while the robot is climbing up slopes with different inclination angles. The robot finally drops at 7° slope, setting a limit for its climbing capacity. The climbing motion is illustrated in Figure 3d and is shown in real time in Movie S5 (Supporting Information). It is also important to note that the wavelength used for actuation (450–550 nm) and the moderate intensity (hundreds of mW cm^{-2}) are both human safe. Therefore, the robot is able to perform the rolling movement even on human skin. As a glimpse to the future, Figure 3f shows the robot starts to translocate on a human hand (also see Movie S6, Supporting Information), showing the opportunity of developing human-friendly platform for human–robot interaction.

In the past decades, photoalignment technique has attained great interest in the LCN community,[49,50] enabling to obtain complex molecular alignment patterns and versatile 2D-to-3D shape-morphing in LCN films. Photopatterning paves way toward origami robotics, which offers many advantages such as automation and space saving, but precise control over the shape-morphing geometry in soft matter is always challenging. Kirigami serves as an alternative platform for obtaining 3D shape-morphing, with the help of applying an external force (stress field), when the material is not actuated. The kirigami method provides good controllability of the 3D shape-morphing through applying forces, while the principle can be easily extended to other film-like actuators such as carbon bilayers,[6] shape-memory alloys,[31] etc. Figure S11 (Supporting Information) shows kirigami patterns inscribed on a polymer–aluminum bilayer actuator and their thermal actuation behavior, indicating that the presented concept can be generalized to different types of stimuli-responsive materials.

The interplay between intrinsic materials properties and the external stimuli can lead to intriguing phenomena in soft materials, such as self-oscillation,[21,51] wave-like self-propelling[52] and various forms of self-sustained motion.[52–55] Those phenomena are initiated by an in-built feedback mechanism connecting the material response, stimulus fields, and the structural geometry.[21] One example is the wave-like self-oscillation implemented by an LCN strip under a compressing stress field[52] and it is similar as that observed in snapping motions in between a two-wall confinement.[56] Herein, we expect complex architectures induced by 3D kirigami under external stress

fields, would trigger novel design principles in microrobotics and lead to ever-more advanced functional autonomous devices.

In summary, we apply the kirigami concept in a photo-responsive LCN film actuator to achieve different 2D-to-3D shape-changes, induced by external stress fields via stretching, twisting, and bending. We demonstrate light-controlled actuation in the kirigami structures and fabricate a kirigami rolling robot with multiple photomechanical petals. The robot is able to perform multigait rolling movement in both forward and backward direction, with capabilities that are unreachable by conventional light driven rolling devices. The robot can be steered with light along predesigned 2D trajectories, and it can climb up a slope up to 6°. Kirigami serves as an efficient technique to obtain 2D-to-3D shape-morphing in generally flat materials like films and sheets. Although easy to process, the obtained architectures are passive. Photomechanical materials contain intrinsic features of active deformability upon light stimuli, but obtaining 3D constructions of such materials prior to actuation stage is still challenging. The results presented in this work are an attempt to cross boundaries by combining kirigami technique and photomechanical materials, suggesting a facile technique to fabricate complex geometries in responsive films, and may provide unforeseen inspiration for both kirigami devices and soft microrobotics.

Experimental Section

Materials: The LCN actuator is made by photopolymerization of a mixture that contains 78 mol% of LC monomer 4-methoxybenzoic acid 4-(6-acryloyloxyhexyloxy)phenyl ester, 20 mol% of LC crosslinker 1,4-bis-[4-(3-acryloyloxypropyloxy)benzoyloxy]-2-methylbenzene (both purchased from Synthon chemicals), 1 mol% of light-responsive molecule *N*-ethyl-*N*-(2-hydroxyethyl)-4-(4-nitrophenylazo)aniline (Disperse Red 1, Sigma Aldrich), and 1 mol% of photoinitiator (2,2-dimethoxy-2-phenylacetophenone, Sigma Aldrich). All molecules were used as received.

Film Fabrication: Glass substrates were cleaned by sonication in acetone bath for 20 min and dried under nitrogen flow. A glass slide was spin coated with 0.1 wt% water solution of poly(vinyl alcohol) (PVA, Sigma Aldrich; 4000 RPM, 1 min), dried at 100 °C on a hot plate for 10 min, and rubbed unidirectionally using a satin cloth. After rubbing, the PVA-coated substrates were blown with high-pressure nitrogen to remove dust from the surfaces. Another glass slide was spin coated with homeotropic alignment layer (Olink Technology Co., Ltd, 4000 RPM, 1 min), and baked at 100 °C for 10 min and 180 °C for 30 min. The two coated substrates were fixed together with UV glue (FP-32, DaJiun), using spacer particles (50 µm) to define the cell thickness. The mixture was then infiltrated into the cell on a heating stage at 80 °C and cooled down to 45 °C with a rate of 3 °C min^{-1}. An LED (385 nm, 57 mW cm^{-2}, 5 min) was used to polymerize the LC mixture.

Kirigami and Robot Fabrication: The cut patterns were designed using Adobe Illustrator and sent to laser cutter (FLUX Beambox Pro, CO_2 laser, 50 W) for engraving structures onto the splay-aligned LCN films. The LCN-coated substrates were dipped into water, and the cut films were detached from the substrate by using a blade. To fabricate the robot, the cut film was rolled up into a tube-like structure and fixed by using drops of UV curable glue. The structure consists of ten pairs of LCN petal, each is 2.5 mm long and around 1 mm wide. Details about kirigami design, macroscopic image of laser cut film and microscopic image of the cut edge can be seen in Figure S12 (Supporting Information). A plastic tube cropped from a straw (4 mm in diameter, 100 µm thick) was set in the middle, yielding an eventual device of 10 mg weight. The plastic tube was used to reinforce the structure, thus preventing the deformation in diameter and damage of the fragile film upon light illumination. Photos of photoactuation in a robot without reinforcement are shown in Figure S13 (Supporting Information).

Tracking of the Robot: The tracking position of the rolling robot was recorded by using a function "IMFINDCIRCLES" in MATLAB (R2019a). The recorded videos (side-view, 120 frames s^{-1}) were converted into series images that were converted from RGB to grayscale to facilitate the software analysis. Circular edges of the robot ring were detected by the program in every image, and the tracking position (the center of mass) was determined by the center of the circle. The position tracking stopped when the robot reached a moving distance of 25 mm in horizontal direction, due to the traveling limit of the motorized stage.

Rolling Distance Statistics: The horizontal rolling distance (center of mass), d, was compared with the steady moving distance of the scanning spot, d_s, by $\Delta d = d - d_s$. Δd was recorded in every frame of image during the entire movement (20 frame s^{-1}), for different light illumination conditions, e.g., scanning speed: 1– 6 mm s^{-1} and incident angle: 10–40°. The mean Δd and the standard division present the consistence of movement between the rolling robot and the driving spot. For example, a slight negative value of Δd means a small lag back of the movement compared to the spot position, and a large standard division means a failure of light driven motion, in which the robot could not catch up the speed of the spot.

Supporting Information

Supporting Information is available from the Wiley Online Library or from the author.

Acknowledgements

This work was financially supported from the Young Scholar Fellowship Program by Ministry of Science and Technology (MOST) in Taiwan (Grant MOST108-2636-M-027-001), European Research Council (ERC Starting Grant PHOTOTUNE, no. 679646) and Academy of Finland (postdoctoral grant no. 326445). This work is part of the Academy of Finland Flagship Programme "Photonics Research and Innovation (PREIN)," Decision Number 320165.

Conflict of Interest

The authors declare no conflict of interest.

Keywords

actuation, kirigami, light steering, liquid crystal network, soft robots

Received: September 23, 2019
Revised: October 28, 2019
Published online:

[1] D. Rus, M. T. Tolley, *Nature* **2015**, *521*, 467.
[2] S. Song, M. Sitti, *Adv. Mater.* **2014**, *26*, 4901.
[3] G. M. Whitesides, *Angew. Chem., Int. Ed.* **2018**, *57*, 4258.
[4] S. Palagi, P. Fischer, *Nat. Rev. Mater.* **2018**, *3*, 113.
[5] H. Zeng, P. Wasylczyk, D. S. Wiersma, A. Priimagi, *Adv. Mater.* **2018**, *30*, 1703554.
[6] Y. Hu, J. Liu, L. Chang, L. Yang, A. Xu, K. Qi, P. Lu, G. Wu, W. Chen, Y. Wu, *Adv. Funct. Mater.* **2017**, *27*, 1704388.

[7] T. Ikeda, J.-I. Mamiya, Y. Yu, *Angew. Chem., Int. Ed.* **2007**, *46*, 506.
[8] H. Lee, C. Xia, N. X. Fang, Soft Matter, *Soft Matter* **2010**, *6*, 4342.
[9] W. Hu, G. Z. Lum, M. Mastrangeli, M. Sitti, *Nature* **2018**, *554*, 81.
[10] K. Y. MA, P. Chirarattananon, S.B. Fuller, R. J. Wood, *Science* **2013**, *340*, 603.
[11] R. F. Shepherd, F. Ilievski, W. Choi, S. A. Morin, A. A. Stokes, A. D. Mazzeo, X. Chen, M. Wang, G. M. Whitesides, *Proc. Natl. Acad. Sci. USA* **2011**, *108*, 20400.
[12] T. Qiu, T. C. Lee, A. G. Mark, K. I. Morozov, R. Münster, O. Mierka, S. Turek, A. M. Leshansky, P. Fischer, *Nat. Commun.* **2014**, *5*, 5119.
[13] H. Zhang, A. Mourran, M. Möller, *Nano Lett.* **2017**, *17*, 2010.
[14] J. Li, R. Zhang, L. Mou, M. Andrade, H. Hu, K. Yu, J. Sun, T. Jia, Y. Dou, H. Chen, M. Zhang, D. Qian, Z. Liu, *Adv. Funct. Mater.* **2019**, *29*, 1808995.
[15] A. A. Solovev, W. Xi, D. H. Gracias, S. M. Harazim, C. Deneke, S. Sanchez, O. G. Schmidt, *ACS Nano* **2012**, *6*, 1751.
[16] T. V. Manen, S. Janbaz, A. A. Zadpoor, *Mater. Today* **2018**, *21*, 144.
[17] T. J. White, D. J. Broer, *Nat. Mater.* **2015**, *14*, 1087.
[18] C. Ohm, M. Brehmer, R. Zentel, *Adv. Mater.* **2010**, *22*, 3366.
[19] S. J. Aßhoff, F. Lancia, S. Iamsaard, B. Matt, T. Kudernac, S.P. Fletcher, N. Katsonis, *Angew. Chem., Int. Ed.* **2017**, *56*, 3261.
[20] B. Zuo, M. Wang, B. P. Lin, H. Yang, *Chem. Mater.* **2018**, *30*, 8079.
[21] X. Q. Wang, C. F. Tan, K. H. Chan, X. Lu, L. Zhu, S. W. Kim, G. W. Ho, *Nat. Commun.* **2018**, *9*, 3438.
[22] R. R. Kohlmeyer, J. Chen, *Angew. Chem., Int. Ed.* **2013**, *52*, 9234.
[23] M. Rogóż, H. Zeng, C. Xuan, D. S. Wiersma, P. Wasylczyk, *Adv. Opt. Mater.* **2016**, *4*, 1689.
[24] S. Palagi, A. Mark, S. Y. Reigh, K. Melde, T. Qiu, H. Zeng, C. Parmeggiani, D. Martella, A. Sanchez-Castillo, N. Kapernaum, F. Giesselmann, D. S. Wiersma, E. Lauga, P. Fischer, *Nat. Mater.* **2016**, *15*, 647.
[25] M. Rogóż, K. Dradrach, C. Xuan, P. Wasylczyk, *Macromol. Rapid Commun.* **2019**, *40*, 1900279.
[26] H. Zeng, P. Wasylczyk, C. Parmeggiani, D. Martella, M. Burresi, D. S. Wiersma, *Adv. Mater.* **2015**, *27*, 3883.
[27] C. P. Ambulo, J. J. Burroughs, J. M. Boothby, H. Kim, M. R. Shankar, T. H. Ware, *ACS Appl. Mater. Interfaces* **2017**, *9*, 37332.
[28] M. López-Valdeolivas, D. Liu, D. J. Broer, C. Sánchez-Somolinos, *Macromol. Rapid Commun.* **2018**, *39*, 1700710.
[29] J. L. Silverberg, J. H. Na, A. A. Evans, B. Liu, T. C. Hull, C. D. Santangelo, R. J. Lang, R. C. Hayward, I. Cohen, *Nat. Mater.* **2015**, *14*, 389.
[30] Y. Liu, J. Genzer, M. D. Dickey, *Prog. Polym. Sci.* **2016**, *52*, 79.
[31] Y. Liu, B. Shaw, M. D. Dickey, J. Genzer, *Sci. Adv.* **2017**, *3*, e1602417.
[32] J. Ryu, M. D'Amato, X. Cui, K. N. Long, H. Jerry Qi, M. L. Dunn, *Appl. Phys. Lett.* **2012**, *100*, 161908.
[33] J. L. Silverberg, A. A. Evans, L. McLeod, R. C. Hayward, T. Hull, C. D. Santangelo, I. Cohen, *Science* **2014**, *345*, 647.
[34] L. Xu, T. C. Shyu, N. A. Kotov, *ACS Nano* **2017**, *11*, 7587.
[35] J. H. Na, A. A. Evans, J. Bae, M. C. Chiappelli, C. D. Santangelo, R. J. Lang, T. C. Hull, R. C. Hayward, *Adv. Mater.* **2015**, *27*, 79.
[36] P. V. Gimenez, F. Ye, B. Mbanga, J. V. Selinger, R. L. B. Selinger, *Sci. Rep.* **2017**, *7*, 45370.
[37] Y. Tang, G. Lin, S. Yang, Y. K. Yi, R. D. Kamien, J. Yin, *Adv. Mater.* **2017**, *29*, 1604262.
[38] A. Rafsanjani, Y. Zhang, B. Liu, S. M. Rubinstein, K. Bertoldi, *Sci. Rob.* **2018**, *3*, eaar7555.
[39] C. D. Modes, M. Warner, C. Sanchez-Somolinos, L. T. de Haan, D. Broer, *Proc. R. Soc. A* **2013**, *469*, 20120631.
[40] J. A. Lv, Y. Liu, J. Wei, E. Chen, L. Qin, Y. Yu, *Nature* **2016**, *537*, 179.
[41] X. Qian, Q. Chen, Y. Yang, Y. Xu, Z. Li, Z. Wang, Y. Wu, Y. Wei, Y. Ji, *Adv. Mater.* **2018**, *30*, 1801103.
[42] M. Babaei, J. A. Clement, K. Dayal, M. R. Shankar, *RSC Adv.* **2017**, *7*, 52510.
[43] X. Lu, H. Zhang, G. Fei, B. Yu, X. Tong, H. Xia, Y. Zhao, *Adv. Mater.* **2018**, *30*, 1706597.
[44] L. T. De Haan, C. Sánchez-Somolinos, C. M. W. Bastiaansen, A. P. H. J. Schenning, D. J. Broer, *Angew. Chem., Int. Ed.* **2012**, *51*, 12469.
[45] O. M. Wani, H. Zeng, A. Priimagi, *Nat. Commun.* **2017**, *8*, 15546.
[46] H. Zeng, O. M. Wani, P. Wasylczyk, R. Kaczmarek, A. Priimagi, *Adv. Mater.* **2017**, *29*, 1701814.
[47] M. Yamada, M. Kondo, J. I. Mamiya, Y. Yu, M. Kinoshita, C. J. Barrett, T. Ikeda, *Angew. Chem., Int. Ed.* **2008**, *47*, 4986.
[48] X. Lu, S. Guo, X. Tong, H. Xia, Y. Zhao, *Adv. Mater.* **2017**, *29*, 1606467.
[49] T. Seki, *Polym. J.* **2014**, *46*, 751.
[50] O. Yaroshchuk, Y. Reznikov, *J. Mater. Chem.* **2012**, *22*, 286.
[51] T. J. White, N. V. Tabiryan, S. V. Serak, U. A. Hrozhyk, V. P. Tondiglia, H. Koerner, R. A. Vaia, T. J. Bunning, *Soft Matter* **2008**, *4*, 1796.
[52] A. H. Gelebart, D. Jan Mulder, M. Varga, A. Konya, G. Vantomme, E. W. Meijer, R. L. B. Selinger, D. J. Broer, *Nature* **2017**, *546*, 632.
[53] J. J. Wie, M. R. Shankar, T. J. White, *Nat. Commun.* **2016**, *7*, 13260.
[54] A. Baumann, A. Sánchez-Ferrer, L. Jacomine, P. Martinoty, V. Le Houerou, F. Ziebert, I. M. Kulić, *Nat. Mater.* **2018**, *17*, 523.
[55] C. Ahn, K. Li, S. Cai, *ACS Appl. Mater. Interfaces* **2018**, *10*, 25689.
[56] M. R. Shankar, M. L. Smith, V. P. Tondiglia, K. M. Lee, M. E. McConney, D. H. Wang, L. S. Tan, T. J. White, *Proc. Natl. Acad. Sci. USA* **2013**, *110*, 18792.